

Photoproduction of axion-like particles

Daniel Aloni,^{1,*} Cristiano Fanelli,^{2,†} Yotam Soreq,^{3,4,‡} and Mike Williams^{2,§}

¹*Department of Particle Physics and Astrophysics,
Weizmann Institute of Science, Rehovot, Israel 7610001*

²*Laboratory for Nuclear Science, Massachusetts Institute of Technology, Cambridge, MA 02139, U.S.A.*

³*Theoretical Physics Department, CERN, CH-1211 Geneva 23, Switzerland*

⁴*Department of Physics, Technion, Haifa 32000, Israel*

We explore the sensitivity of photon-beam experiments to axion-like particles (ALPs) with QCD-scale masses whose dominant coupling to the Standard Model is either to photons or gluons. We introduce a novel data-driven method that eliminates the need for knowledge of nuclear form factors or the photon-beam flux when considering coherent Primakoff production off a nuclear target, and show that data collected by the PRIMEX experiment could substantially improve the sensitivity to ALPs with $0.03 \lesssim m_a \lesssim 0.3 \text{ GeV}$. Furthermore, we explore the potential sensitivity of running the GLUEX experiment with a nuclear target and its planned PRIMEX-like calorimeter. For the case where the dominant coupling is to gluons, we study photoproduction for the first time, and predict the future sensitivity of the GLUEX experiment using its nominal proton target. Finally, we set world-leading limits for both the ALP-gluon coupling and the ALP-photon coupling based on public mass plots.

Axion-like particles (ALPs) are hypothetical pseudoscalars found in many proposed extensions to the Standard Model (SM), since they naturally address the Strong CP [1–4] and Hierarchy problems [5]. Furthermore, ALPs may explain the muon magnetic moment anomaly [6, 7], and could connect SM particles to dark matter by providing a *portal* [8–11]. The couplings of ALPs to the SM are highly suppressed at low energies by a large cut-off scale Λ ; however, since ALPs, a , are pseudo-Nambu-Goldstone bosons, their mass (m_a) can be much smaller than the scale that controls their dynamics, *i.e.* $m_a \ll \Lambda$. Recently, ALPs with MeV-to-GeV scale masses, henceforth QCD scale, have received considerable interest [7, 12–23] (see, in addition, Refs.[24–28] for recent ALP reviews).

In this Letter, we explore the discovery potential of photon-beam experiments for ALPs with QCD-scale masses. Specifically, we consider two cases: ALPs whose dominant coupling to SM particles is to photons or to gluons. For the former, the best sensitivity involves coherent Primakoff production off a nuclear target (see Fig. 1 top). While ALP production using the Primakoff process has been studied before [7, 29], our work is novel in three aspects: (i) we introduce a fully data-driven ALP normalization method, which eliminates the need for knowledge of nuclear form factors or the photon-beam flux; (ii) we show that data collected by the PRIMEX experiment at Jefferson Lab could substantially improve the sensitivity to ALPs with $0.03 \lesssim m_a \lesssim 0.3 \text{ GeV}$, in fact, we are able to set world-leading limits from a diphoton mass plot published in Ref. [30] from a sin-

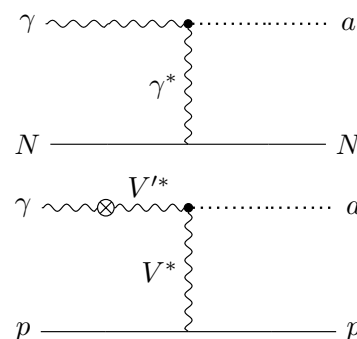


FIG. 1: (top) Primakoff production via t -channel photon exchange, and (bottom) photoproduction via photon-vector-meson mixing and t -channel vector-meson exchange.

gle angular bin; and (iii) we explore for the first time the potential sensitivity of running the GLUEX experiment at Jefferson Lab with a nuclear target and its planned PRIMEX-like calorimeter. For the case where the dominant SM coupling of ALPs is to gluons, we extend our work in Ref. [31] and study photoproduction for the first time. The dominant photoproduction mechanism is photon-vector-meson mixing and t -channel vector-meson exchange (see Fig. 1 bottom). We obtain the future sensitivity of the GLUEX experiment using its nominal proton target, and set world-leading limits based on a public mass plot.

The effective Lagrangian describing the interactions of ALPs with photons and gluons is

$$\mathcal{L}_{\text{eff}} \supset \frac{c_\gamma}{4\Lambda} a F^{\mu\nu} \tilde{F}_{\mu\nu} - \frac{4\pi\alpha_s c_g}{\Lambda} a G^{\mu\nu} \tilde{G}_{\mu\nu}, \quad (1)$$

where $F_{\mu\nu}$ ($G_{\mu\nu}$) is the photon (gluon) field strength tensor with $\tilde{F}_{\mu\nu} = \frac{1}{2}\epsilon_{\mu\nu\alpha\beta} F^{\alpha\beta}$ ($\tilde{G}_{\mu\nu}$ satisfies a similar expression). Our approach to studying ALP-hadron interactions follows Refs. [32–34], and we take the ALP-

*Electronic address: daniel.aloni@weizmann.ac.il

†Electronic address: cfanelli@mit.edu

‡Electronic address: yotam.soreq@cern.ch

§Electronic address: mwill@mit.edu

pseudoscalar mixing, along with the ALP lifetime and branching fractions, directly from Ref. [31]. The two scenarios considered in this Letter correspond to $c_g = 0$, $c_\gamma = 1$ and $c_g = 1$, $c_\gamma = 0$; however, we stress that our results can be generalized to any other set of ALP couplings to the SM particles (see Ref. [31]).

First, we consider the case where the dominant ALP-SM coupling is to photons. When a photon beam is incident on a nuclear target, the production of pseudoscalars—either the mesons $P = \pi^0, \eta$ or ALPs—at forward angles is dominantly via the coherent Primakoff process for $m_{a,P} \lesssim 1$ GeV. The differential cross section for elastic coherent Primakoff production from a nucleus, N , is given by

$$\frac{d\sigma_{\gamma N \rightarrow a N}^{\text{elastic}}}{dt} = \alpha Z_N^2 F_N^2(t) \Gamma_{a \rightarrow \gamma\gamma} \mathcal{H}(m_N, m_a, s, t), \quad (2)$$

where t and s are the Mandelstam variables, F_N is the nuclear form factor (see the Supplemental Material [35] to this Letter and Refs. [36–38]), $\Gamma_{a \rightarrow \gamma\gamma} = c_\gamma^2 m_a^3 / (64\pi\Lambda^2)$ is the partial decay width of the decay $a \rightarrow \gamma\gamma$, and

$$\mathcal{H}(m_N, m_a, s, t) \equiv 128\pi \frac{m_N^4}{m_a^3} \times \frac{m_a^2 t (m_N^2 + s) - m_a^4 m_N^2 - t((s - m_N^2)^2 + st)}{t^2 (s - m_N^2)^2 (t - 4m_N^2)^2}. \quad (3)$$

For pseudoscalar mesons, the corresponding differential cross section is obtained by the replacement $a \rightarrow P$.

For small values of t (forward angles), where elastic coherent Primakoff production is dominant, the nuclear form factor dependence can be canceled by forming the ratio of the ALP and P differential cross sections as follows:

$$\frac{d\sigma_{\gamma N \rightarrow a N}^{\text{elastic}}}{dt} = \frac{\Gamma_{a \rightarrow \gamma\gamma}}{\Gamma_{P \rightarrow \gamma\gamma}} \frac{\mathcal{H}(m_N, m_a, s, t)}{\mathcal{H}(m_N, m_P, s, t)} \frac{d\sigma_{\gamma N \rightarrow P N}^{\text{elastic}}}{dt}. \quad (4)$$

Therefore, the ALP yield—up to a factor of the model parameters $(c_\gamma/\Lambda)^2$ —can be determined from the observed π^0 and/or η Primakoff yields, making this a completely data-driven search. The nuclear form factor does not need to be known, and the photon flux also cancels using our approach. A correction must be applied to account for any mass dependence in the detector efficiency at fixed t and s , though this should be easy to obtain from simulation given that the $a \rightarrow \gamma\gamma$ decay distribution is known (it must be uniform in the a rest frame). Finally, we note that quasi-elastic ALP Primakoff production can be estimated using a similar approach; however, this production mechanism is negligible in the m_a range considered here (see the Supplemental Material [35]).

The first run of the PRIMEX experiment was in Hall B at Jefferson Lab in 2004 [30]. Data were collected on both C and Pb targets using a 4.9–5.5 GeV photon beam and a high-resolution multichannel calorimeter, which allowed PRIMEX to make the most precise measurement to date of the $\pi^0 \rightarrow \gamma\gamma$ decay width. The integrated luminosities

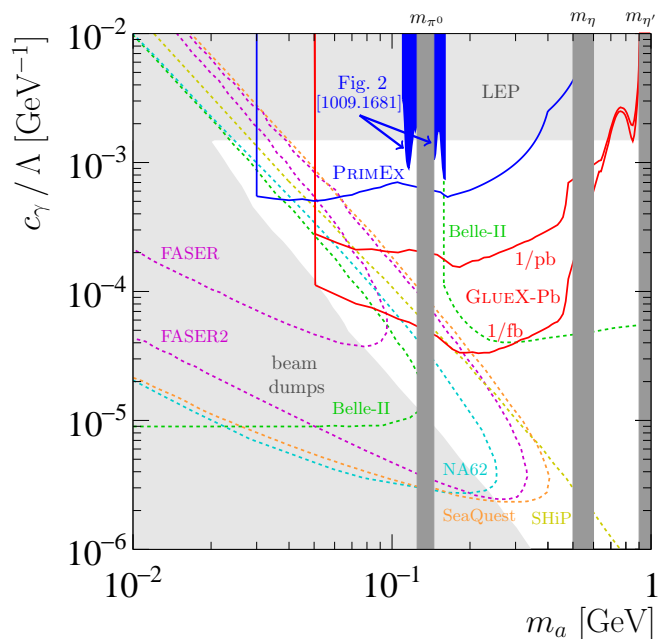


FIG. 2: The PRIMEX (blue) and GLUEX (red) projections for the ALP-photon coupling ($c_\gamma = 1$, $c_g = 0$) compared to the current bounds [15, 39–41] and projections of NA62, SeaQuest, Belle 2, SHiP and FASER [13, 42–44]. In addition, a new limit is set (dark blue shaded regions) using the published $m_{\gamma\gamma}$ spectrum from one angular bin of carbon-target PRIMEX data from Fig. 2 of Ref. [30].

were 0.3/pb for C and 0.002/pb for Pb. A follow-up run of PRIMEX was performed in 2010, which collected 0.4/pb on C and 0.3/pb on Si, though only preliminary results have been produced thus far from this data set.

Reference [30] published the diphoton mass spectrum near the π^0 peak for one forward angular bin from the C data obtained in the first PRIMEX run (see Fig. 2 of Ref. [30]). The diphoton efficiency is roughly constant within such a small angular and mass window; therefore, using the observed π^0 yield in the published peak (≈ 5100) and the background yield at each $m_{\gamma\gamma}$, we can use Eq. (4) to place constraints on Λ for $c_\gamma = 1$ and $c_g = 0$. For example, at $m_a = 0.11$ GeV the background in a $\pm 2\sigma$ window is ≈ 300 giving a rough estimate of the sensitivity to the ALP yield of $\approx 2\sqrt{300}$. Using Eq. (4) we estimate this corresponds to $\Lambda \approx 0.6$ TeV, which is comparable to the world-leading constraint from LEP at this mass [15, 39]. In the Supplemental Material [35], we perform a more rigorous study of this spectrum, the results of which are shown in Fig. 2 and confirm that this small fraction of the PRIMEX data sample provides competitive sensitivity to LEP—and even gives world-leading constraints at a few masses.

To estimate the sensitivity of each PRIMEX data sample, *i.e.* not just the one bin shown in Fig. 2 of Ref. [30], we need to determine the mass dependence of the efficiency and to estimate the background versus $m_{\gamma\gamma}$ in each sample. A detailed description of this part of the

analysis is provided in the Supplemental Material [35], and briefly summarized here. We assume that the same selection criteria applied in Ref. [30] are used for the ALP search and take the PRIMEX calorimeter acceptance and resolution from Refs. [45, 46]. Furthermore, we assume that the ALP bump hunt will only use candidates with $\theta_{\gamma\gamma} < 0.5^\circ$, where π^0 production is dominated by the Primakoff process for all targets.

Using the known nuclear form factors and Primakoff differential cross section [47–49], we generate Primakoff π^0 Monte Carlo events for the PRIMEX photon-beam energy. We require that both photons from the $\pi^0 \rightarrow \gamma\gamma$ decay are in the PRIMEX calorimeter fiducial acceptance region [30] and apply the required smearing to account for resolution. The width of our Monte Carlo π^0 peak is consistent with the data in Ref. [30]. We then apply the full selection of Ref. [30] and find that our predicted π^0 Primakoff yields are consistent with those observed in Refs. [50, 51]. We assume that the reconstruction efficiency is independent of the ALP mass in the search region (excluding geometrical acceptance effects). In addition, we discard the low- m_a region where the photon clusters begin to overlap and the acceptance has strong mass dependence. Lower masses can likely be explored in an analysis of the actual PRIMEX data with access to a full detector simulation.

As in any bump hunt, obtaining a data-driven background estimate is straightforward using the $m_{\gamma\gamma}$ sidebands at each m_a (see, *e.g.*, Refs. [52, 53]). However, estimating the background without the data is considerably more difficult, so we adopt a conservative approach. We considered many possible backgrounds, *e.g.* $\gamma N \rightarrow N\omega(\pi^0[\gamma\gamma]\gamma)$ where one photon is not reconstructed or the π^0 photons are merged into a single cluster, though we found that no hadronic reactions are capable of contributing background at a rate comparable to that observed in Fig. 2 of Ref. [30] in the mass range probed by PRIMEX. Thus, we conclude that the PRIMEX background is dominantly due to electromagnetic interactions of the photon beam with the target that produce either additional photons or e^+e^- pairs. Figure 2 of Ref. [30] shows the forward-most angular region. Given that the beam backgrounds should decrease moving away from the beam line, using this angular bin—and assuming a uniformly distributed background—provides a conservative background estimate. We also conservatively assume that the background density above (below) the $m_{\gamma\gamma}$ region shown in Fig. 2 of Ref. [30] takes on the value at the upper-most (lower-most) bin of the published $m_{\gamma\gamma}$ spectrum. Finally, we scale the beam-induced background, which is shown for the first C run, by the product of the target radiation length and the number of photons on target for other PRIMEX runs.

Our projected sensitivity for the entire PRIMEX data sample is shown in Fig. 2, *i.e.* our estimate combines all of the PRIMEX runs. The PRIMEX sensitivity would be substantially better than LEP for $0.03 \lesssim m_a \lesssim 0.3$ GeV and provide world-leading sensitivity up to

about 0.4 GeV. We stress again that the PRIMEX data are already on tape, and are well calibrated and understood. All that is needed is to perform a bump hunt on the forward-angle data in the region dominated by Primakoff production. Following the approach we proposed above, the normalization can be done in a purely data-driven way using the observed π^0 Primakoff yield differentially versus t .

An updated version of the PRIMEX experiment recently ran in Hall D at Jefferson Lab using the GLUEX detector with an additional small-angle calorimeter [54]. This new experiment has the potential to explore higher masses than PRIMEX due to the higher photon-beam energy of 11 GeV and the larger acceptance of the GLUEX forward calorimeter; however, the use of a helium target in this new run makes it less sensitive than PRIMEX for ALPs. There are several proposals for future GLUEX running with heavy nuclear targets [55], so it is interesting to explore the potential sensitivity to ALPs of such runs. Specifically, we consider a Pb target here. We take the GLUEX acceptance, efficiency, and resolution from Refs. [56, 57], and the corresponding values for the small-angle calorimeter from Ref. [54]. For $m_a < m_\eta$, we rescale the expected beam background from the PRIMEX Pb run. There are three additional backgrounds that contribute to the GLUEX run at higher masses: Primakoff production of η and η' mesons, and coherent nuclear production of $\gamma N \rightarrow N\omega(\pi^0[\gamma\gamma]\gamma)$ (as described above). The cross sections for these processes are well known, making it straightforward to estimate their yields using Monte Carlo.

An additional complication arises when projecting the sensitivity of GLUEX. The GLUEX experiment could explore regions of ALP parameter space where the ALP flight distance becomes nonnegligible. Using Monte Carlo, we estimate that the impact on the ALP mass resolution and acceptance is small provided that its lab-frame flight distance is $\lesssim 30$ cm (the length of the nominal liquid hydrogen target cell). For simplicity, we apply a fiducial cut on the flight distance at 30 cm, which is conservative since ALPs that decay after this distance could still be detected and a detailed study could determine the appropriate signal shape for each value of Λ . Our estimate of the projected reach for GLUEX including the PRIMEX-like calorimeter is shown in Fig. 2. The larger data set assumes that as much data is collected as is expected in the full GLUEX proton-target run. The smaller data set corresponds to collecting 1/pb of Pb-target data.

Figure 2 shows that Primakoff production using photon beams can provide unique sensitivity to ALPs. The data from PRIMEX, which has been on tape for a decade, could provide substantially better sensitivity than LEP for $0.03 \lesssim m_a \lesssim 0.3$ GeV. Running the GLUEX experiment for a few years with a Pb target and its PRIMEX-like small-angle calorimeter could explore the remaining parameter space down to where future beam-dump experiments will have sensitivity. Much of this parameter space is not accessible at any other current or proposed

future experiment.

We now move on to considering the case where the dominant ALP-SM coupling is to gluons. In this scenario, nuclear targets do not provide a large advantage since both the signal and background scale similarly with the number of nucleons, so we consider the nominal liquid-hydrogen target and default experimental GLUEX setup, which has been running for the past few years. When a photon beam is incident on a proton target, exclusive pseudoscalar production is dominantly via photon-vector-meson mixing as shown in Fig. 1 bottom. In the Supplemental Material [35], we show that—once both π^0 and η photoproduction are well understood—it is possible to derive a fully data-driven normalization strategy similar to the one we proposed above for Primakoff production. As discussed in Ref. [58], η production at GLUEX energies, while clearly dominantly t -channel, is not yet fully understood. Therefore, we will adopt a simplified approach below, though we do provide a complete description of how to implement the fully data-driven strategy for future searches in the Supplemental Material [35].

In principle, ALP searches at GLUEX could look for hadronic final states like $a \rightarrow 3\pi$ and $a \rightarrow \eta\pi\pi$; however, we studied these and found that the mass resolution at GLUEX makes ALP peaks comparable in width to $\omega, \eta', \phi \rightarrow 3\pi$ and $\eta', f_2 \rightarrow \eta\pi\pi$ making it likely that large mass regions need to be vetoed in such searches. Furthermore, the sensitivity at higher masses would not be competitive with b -hadron decays [31]. Therefore, we choose to focus on the $a \rightarrow \gamma\gamma$ decay in the region between the π^0 and η mesons, where its branching fraction is close to unity and diphoton backgrounds are small. Since $a \rightarrow \pi\pi$ and $a \rightarrow \pi^0\gamma$ are forbidden by CP and C , respectively, the $a \rightarrow \gamma\gamma$ decay is dominant in all ALP models in most of this mass region.

For $m_{\pi^0} < m_a < m_\eta$, the ALP-gluon coupling can be replaced by ALP-pseudoscalar-meson mixing by performing a chiral transformation of the light-quark fields [32–34]. Following Ref. [31], we denote the mixing of the ALP with the π^0 and η as $\langle a\pi^0 \rangle$ and $\langle a\eta \rangle$, respectively, and we take these m_a -dependent mixings directly from Ref. [31]. For $|t| \lesssim 1 \text{ GeV}^2$ in this m_a region, at fixed s and t the following approximation is valid to $\mathcal{O}(1)$, which is roughly the same fidelity with which the ALP-pseudoscalar mixing terms are known:

$$\frac{d\sigma_{\gamma p \rightarrow ap}}{dt} \approx \left(\frac{f_\pi}{f_a}\right)^2 \times \left[|\langle a\pi^0 \rangle|^2 \frac{d\sigma_{\gamma p \rightarrow \pi^0 p}}{dt} + |\langle a\eta \rangle|^2 \frac{d\sigma_{\gamma p \rightarrow \eta p}}{dt} \right], \quad (5)$$

where f_π and $f_a = \Lambda/(32\pi^2 c_g)$ are the pion and ALP decay constants. This approximation works well in this mass range due to the dominance of the contributions from π^0 or η mixing to the ALP $U(3)$ representation. We adopt the relevant numerical values from Refs. [59–61], see Supplemental Material for details.

Ref. [58] published the $m_{\gamma\gamma}$ spectrum, along with the yields and efficiencies versus t of both the π^0 and η mesons. In the Supplemental Material, we perform a bump hunt of the $m_{\gamma\gamma}$ spectrum to obtain upper limits on the ALP yield at each m_a . The expected ALP yield in a small bin of $[s, t]$ is related to Λ (or f_a) using Eq. (5) according to

$$n_a(s, t) \approx \left(\frac{f_\pi}{f_a}\right)^2 \left[|\langle a\pi^0 \rangle|^2 \frac{n_{\pi^0}(s, t)\epsilon(m_a, s, t)}{\mathcal{B}(\pi^0 \rightarrow \gamma\gamma)\epsilon(m_\pi, s, t)} + |\langle a\eta \rangle|^2 \frac{n_\eta(s, t)\epsilon(m_a, s, t)}{\mathcal{B}(\eta \rightarrow \gamma\gamma)\epsilon(m_\eta, s, t)} \right] \mathcal{B}(a \rightarrow \gamma\gamma), \quad (6)$$

where ϵ denotes the product of the detector acceptance and efficiency. We linearly interpolate the efficiencies given in Ref. [58] at m_{π^0} and m_η for m_a , and confirm this approach is valid to $\mathcal{O}(10\%)$ using toy Monte Carlo as described in the Supplemental Material [35] (additionally, the same ALP lifetime correction is applied here, though this is a small correction). The total expected ALP yield is simply the sum of $n_a(s, t)$ over all bins. By comparing the expected ALP yields to the upper limits obtained from the bump hunt of the $m_{\gamma\gamma}$ spectrum, we place constraints on c_g/Λ (see Fig. 3). These limits are the best over some of the $0.15 < m_a < 0.46 \text{ GeV}$ region. Finally, we also provide the expected sensitivity from a 1/fb GLUEX data set, which is substantially better than any existing limits over most of this mass region.

In summary, we explored the sensitivity of photon-beam experiments to ALPs with QCD-scale masses whose dominant coupling is to either photons or gluons. For the photon-dominant coupling scenario, we introduced a novel data-driven method that eliminates the need for knowledge of nuclear form factors or the photon-beam flux when considering coherent Primakoff production off of a nuclear target, and showed that data collected by PRIMEX could substantially improve the sensitivity to ALPs with $0.03 \lesssim m_a \lesssim 0.3 \text{ GeV}$. We also explored the potential sensitivity of running the GLUEX experiment with a nuclear target. For the case where the dominant coupling is to gluons, we studied photoproduction for the first time, and predicted the future sensitivity of the GLUEX experiment using its nominal proton target. For both scenarios, we set world-leading limits based on public mass plots.

Acknowledgments

We thank Bill Donnelly, Liping Gan, Ashot Gasparian, Or Hen, Ilya Larin, and Michael Spannowsky for useful discussions, as well as Iftah Galon and Sebastian Trojanowski for providing us the details used in Fig. 2 regarding other experiments, and Gilad Perez and Kohsaku Tobioka for pointing out Ref. [64]. YS and MW performed part of this work at the Aspen Center for Physics, which is supported by U.S. National Science Foundation

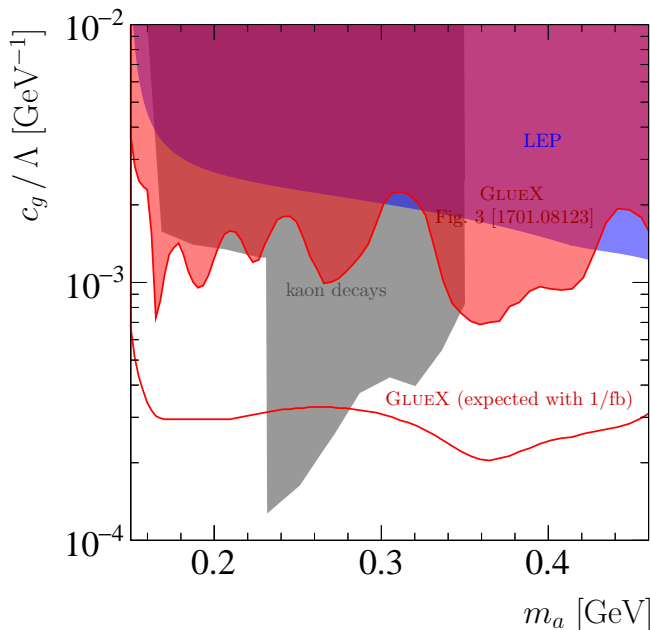


FIG. 3: The GLUEX projection for the ALP-gluon coupling ($c_\gamma = 0$, $c_g = 1$) compared to the current bounds [31] from LEP [15, 39] and kaon decays [14, 62–64]. In addition, a new limit is set using the published $m_{\gamma\gamma}$ spectrum from $\approx 1/\text{pb}$ of GLUEX data from Fig. 3 of Ref. [58].

grant PHY-1607611. This work was supported by: CS and MW were supported by the Office of Nuclear Physics of the U.S. Department of Energy under grant contract number DE-FG02-94ER40818; and MW was also supported by the U.S. National Science Foundation under contract number PHY-1607225.

References

- [1] R. D. Peccei and H. R. Quinn, “CP Conservation in the Presence of Instantons,” *Phys. Rev. Lett.* **38** (1977) 1440–1443. [[328\(1977\)](#)].
- [2] R. D. Peccei and H. R. Quinn, “Constraints Imposed by CP Conservation in the Presence of Instantons,” *Phys. Rev.* **D16** (1977) 1791–1797.
- [3] S. Weinberg, “A New Light Boson?,” *Phys. Rev. Lett.* **40** (1978) 223–226.
- [4] F. Wilczek, “Problem of Strong P and T Invariance in the Presence of Instantons,” *Phys. Rev. Lett.* **40** (1978) 279–282.
- [5] P. W. Graham, D. E. Kaplan, and S. Rajendran, “Cosmological Relaxation of the Electroweak Scale,” *Phys. Rev. Lett.* **115** no. 22, (2015) 221801, [[arXiv:1504.07551 \[hep-ph\]](#)].
- [6] D. Chang, W.-F. Chang, C.-H. Chou, and W.-Y. Keung, “Large two loop contributions to $g-2$ from a generic pseudoscalar boson,” *Phys. Rev.* **D63** (2001) 091301, [[arXiv:hep-ph/0009292 \[hep-ph\]](#)].
- [7] W. J. Marciano, A. Masiero, P. Paradisi, and M. Passera, “Contributions of axionlike particles to lepton dipole moments,” *Phys. Rev.* **D94** no. 11, (2016) 115033, [[arXiv:1607.01022 \[hep-ph\]](#)].
- [8] Y. Nomura and J. Thaler, “Dark Matter through the Axion Portal,” *Phys. Rev.* **D79** (2009) 075008, [[arXiv:0810.5397 \[hep-ph\]](#)].
- [9] M. Freytsis and Z. Ligeti, “On dark matter models with uniquely spin-dependent detection possibilities,” *Phys. Rev.* **D83** (2011) 115009, [[arXiv:1012.5317 \[hep-ph\]](#)].
- [10] M. J. Dolan, F. Kahlhoefer, C. McCabe, and K. Schmidt-Hoberg, “A taste of dark matter: Flavour constraints on pseudoscalar mediators,” *JHEP* **03** (2015) 171, [[arXiv:1412.5174 \[hep-ph\]](#)]. [Erratum: *JHEP*07,103(2015)].
- [11] Y. Hochberg, E. Kuflik, R. McGehee, H. Murayama, and K. Schutz, “SIMP’s through the axion portal,” [[arXiv:1806.10139 \[hep-ph\]](#)].
- [12] J. Jaeckel and M. Spannowsky, “Probing MeV to 90 GeV axion-like particles with LEP and LHC,” *Phys. Lett.* **B753** (2016) 482–487, [[arXiv:1509.00476 \[hep-ph\]](#)].
- [13] B. Dbrich, J. Jaeckel, F. Kahlhoefer, A. Ringwald, and K. Schmidt-Hoberg, “ALPtraum: ALP production in proton beam dump experiments,” *JHEP* **02** (2016) 018, [[arXiv:1512.03069 \[hep-ph\]](#)]. [[JHEP02,018\(2016\)](#)].
- [14] E. Izaguirre, T. Lin, and B. Shuve, “Searching for Axionlike Particles in Flavor-Changing Neutral Current Processes,” *Phys. Rev. Lett.* **118** no. 11, (2017) 111802, [[arXiv:1611.09355 \[hep-ph\]](#)].
- [15] S. Knapen, T. Lin, H. K. Lou, and T. Melia, “Searching for Axionlike Particles with Ultraperipheral Heavy-Ion Collisions,” *Phys. Rev. Lett.* **118** no. 17, (2017) 171801, [[arXiv:1607.06083 \[hep-ph\]](#)].
- [16] A. Mariotti, D. Redigolo, F. Sala, and K. Tobioka, “New LHC bound on low-mass diphoton resonances,” *Phys. Lett.* **B783** (2018) 13–18, [[arXiv:1710.01743 \[hep-ph\]](#)].
- [17] M. Bauer, M. Neubert, and A. Thamm, “Collider Probes of Axion-Like Particles,” *JHEP* **12** (2017) 044, [[arXiv:1708.00443 \[hep-ph\]](#)].
- [18] X. Cid Vidal, A. Mariotti, D. Redigolo, F. Sala, and K. Tobioka, “New Axion Searches at Flavor Factories,” [[arXiv:1810.09452 \[hep-ph\]](#)].
- [19] M. Bauer, M. Heiles, M. Neubert, and A. Thamm, “Axion-Like Particles at Future Colliders,” *Eur. Phys. J.* **C79** no. 1, (2019) 74, [[arXiv:1808.10323 \[hep-ph\]](#)].
- [20] L. Harland-Lang, J. Jaeckel, and M. Spannowsky, “A fresh look at ALP searches in fixed target experiments,” [[arXiv:1902.04878 \[hep-ph\]](#)].
- [21] J. Ebadi, S. Khatibi, and M. Mohammadi Najafabadi, “New Probes for Axion-like Particles at Hadron Colliders,” [[arXiv:1901.03061 \[hep-ph\]](#)].
- [22] K. Mimasu and V. Sanz, “ALPs at Colliders,” *JHEP* **06** (2015) 173, [[arXiv:1409.4792 \[hep-ph\]](#)].
- [23] I. Brivio, M. B. Gavela, L. Merlo, K. Mimasu, J. M. No, R. del Rey, and V. Sanz, “ALPs Effective Field Theory and Collider Signatures,” *Eur. Phys. J.* **C77** no. 8, (2017) 572, [[arXiv:1701.05379 \[hep-ph\]](#)].
- [24] R. Essig *et al.*, “Working Group Report: New Light Weakly Coupled Particles,” in *Proceedings, 2013 Community Summer Study on the Future of U.S. Particle Physics: Snowmass on the Mississippi (CSS2013): Minneapolis, MN, USA, July 29-August 6, 2013*. 2013. [[arXiv:1311.0029 \[hep-ph\]](#)].

- [25] D. J. E. Marsh, “Axion Cosmology,” *Phys. Rept.* **643** (2016) 1–79, [arXiv:1510.07633 \[astro-ph.CO\]](#).
- [26] P. W. Graham, I. G. Irastorza, S. K. Lamoreaux, A. Lindner, and K. A. van Bibber, “Experimental Searches for the Axion and Axion-Like Particles,” *Ann. Rev. Nucl. Part. Sci.* **65** (2015) 485–514, [arXiv:1602.00039 \[hep-ex\]](#).
- [27] I. G. Irastorza and J. Redondo, “New experimental approaches in the search for axion-like particles,” *Prog. Part. Nucl. Phys.* **102** (2018) 89–159, [arXiv:1801.08127 \[hep-ph\]](#).
- [28] J. Beacham *et al.*, “Physics Beyond Colliders at CERN: Beyond the Standard Model Working Group Report,” [arXiv:1901.09966 \[hep-ex\]](#).
- [29] A. Gasparian, “Search for Hidden Sector Scalar Bosons in $X \rightarrow \gamma\gamma$ Channel with Intense Medium Energy Electron Beams,” 2013. <https://axion-wimp2013.desy.de/e201031/e212848/Gasparian.pdf>. 9th PATRAS 2013 workshop, DESY, Hamburg, Germany.
- [30] PrimEx Collaboration, I. Larin *et al.*, “A New Measurement of the π^0 Radiative Decay Width,” *Phys. Rev. Lett.* **106** (2011) 162303, [arXiv:1009.1681 \[nucl-ex\]](#).
- [31] D. Aloni, Y. Soreq, and M. Williams, “Coupling QCD-scale axion-like particles to gluons,” [arXiv:1811.03474 \[hep-ph\]](#).
- [32] H. Georgi, D. B. Kaplan, and L. Randall, “Manifesting the Invisible Axion at Low-energies,” *Phys. Lett.* **169B** (1986) 73–78.
- [33] W. A. Bardeen, R. D. Peccei, and T. Yanagida, “CONSTRAINTS ON VARIANT AXION MODELS,” *Nucl. Phys.* **B279** (1987) 401–428.
- [34] L. M. Krauss and M. B. Wise, “Constraints on Shortlived Axions From the Decay $\pi^+ \rightarrow e^+e^-e^+$ Neutrino,” *Phys. Lett.* **B176** (1986) 483–485.
- [35] See Supplemental Material at XXX for technical details of our calculations and the limit-setting procedures used.
- [36] D. R. Yennie, M. M. Lévy, and D. G. Ravenhall, “Electromagnetic structure of nucleons,” *Rev. Mod. Phys.* **29** (Jan, 1957) 144–157. <https://link.aps.org/doi/10.1103/RevModPhys.29.144>.
- [37] L. N. Hand, D. G. Miller, and R. Wilson, “Alternative nucleon form factors,” *Phys. Rev. Lett.* **8** (Feb, 1962) 110–112. <https://link.aps.org/doi/10.1103/PhysRevLett.8.110>.
- [38] Particle Data Group Collaboration, M. Tanabashi *et al.*, “Review of particle physics,” *Phys. Rev. D* **98** (Aug, 2018) 030001. <https://link.aps.org/doi/10.1103/PhysRevD.98.030001>.
- [39] OPAL Collaboration, G. Abbiendi *et al.*, “Multiphoton production in e^+e^- collisions at $s^{*1/2} = 181\text{--}209\text{ GeV}$,” *Eur. Phys. J.* **C26** (2003) 331–344, [arXiv:hep-ex/0210016 \[hep-ex\]](#).
- [40] J. D. Bjorken, S. Eklund, W. R. Nelson, A. Abashian, C. Church, B. Lu, L. W. Mo, T. A. Nunamaker, and P. Rassmann, “Search for neutral metastable penetrating particles produced in the SLAC beam dump,” *Phys. Rev.* **D38** (1988) 3375.
- [41] J. Blümlein *et al.*, “Limits on neutral light scalar and pseudoscalar particles in a proton beam dump experiment,” *Z. Phys.* **C51** (1991) 341–350.
- [42] J. L. Feng, I. Galon, F. Kling, and S. Trojanowski, “Axionlike particles at FASER: The LHC as a photon beam dump,” *Phys. Rev.* **D98** no. 5, (2018) 055021, [arXiv:1806.02348 \[hep-ph\]](#).
- [43] A. Berlin, S. Gori, P. Schuster, and N. Toro, “Dark Sectors at the Fermilab SeaQuest Experiment,” *Phys. Rev.* **D98** no. 3, (2018) 035011, [arXiv:1804.00661 \[hep-ph\]](#).
- [44] M. J. Dolan, T. Ferber, C. Hearty, F. Kahlhoefer, and K. Schmidt-Hoberg, “Revised constraints and Belle II sensitivity for visible and invisible axion-like particles,” *JHEP* **12** (2017) 094, [arXiv:1709.00009 \[hep-ph\]](#).
- [45] M. Kubantsev, I. Larin, A. Gasparian, and P. Collaboration, “Performance of the primex electromagnetic calorimeter,” in *AIP Conference Proceedings*, vol. 867, pp. 51–58, AIP, 2006.
- [46] I. Larin, D. McNulty, E. Clinton, P. Ambrozewicz, D. Lawrence, I. Nakagawa, Y. Prok, A. Teymurazyan, A. Ahmidouch, A. Asratyan, *et al.*, “new measurement of the π^0 radiative decay width,” *Physical review letters* **106** no. 16, (2011) 162303.
- [47] T. W. Donnelly, J. A. Formaggio, B. R. Holstein, R. G. Milner, and B. Surrow, *Foundations of Nuclear and Particle Physics*. Cambridge University Press, 2017. <http://www.cambridge.org/academic/subjects/physics/particle-physics-and-nuclear-physics/foundations-nuclear-and-particle-physics?format=AR&isbn=9781108110181>.
- [48] W. M. Alberico, A. Molinari, T. W. Donnelly, E. L. Kronenberg, and J. W. Van Orden, “Scaling in electron scattering from a relativistic Fermi gas,” *Phys. Rev.* **C38** (1988) 1801–1810.
- [49] C. W. De Jager, H. De Vries, and C. De Vries, “Nuclear charge and magnetization density distribution parameters from elastic electron scattering,” *Atom. Data Nucl. Data Tabl.* **14** (1974) 479–508. [Erratum: *Atom. Data Nucl. Data Tabl.* 16,580(1975)].
- [50] PRIMEX JLab PAC 33 report: An updated high precision measurement of the neutral pion lifetime via the Primakoff effect.
- [51] Y. Zhang, *A Precision Measurement of Neutral Pion Lifetime*. PhD thesis, Duke University, 2018.
- [52] M. Williams, “Searching for a particle of unknown mass and lifetime in the presence of an unknown non-monotonic background,” *JINST* **10** no. 06, (2015) P06002, [arXiv:1503.04767 \[hep-ex\]](#).
- [53] M. Williams, “A novel approach to the bias-variance problem in bump hunting,” *JINST* **12** no. 09, (2017) P09034, [arXiv:1705.03578 \[hep-ex\]](#).
- [54] A. Gasparian *et al.*, “Update on A Precision Measurement of the η Radiative Decay Width via the Primakoff Effect (pr12-10-011).” 2010.
- [55] M. Dugger *et al.*, “Probing QCD in the nuclear medium with real photons and nuclear targets at GlueX (pr12-17-007).” 2017.
- [56] T. Beattie *et al.*, “Construction and performance of the barrel electromagnetic calorimeter for the GlueX experiment,” *Nuclear Instruments and Methods in Physics Research Section A: Accelerators, Spectrometers, Detectors and Associated Equipment* **896** (2018) 24–42.
- [57] J. M. Hardin, *Upgrading particle identification and searching for leptophobic bosons at GlueX*. PhD thesis, Massachusetts Institute of Technology, 2018.
- [58] GlueX Collaboration, H. Al Ghouli *et al.*, “Measurement of the beam asymmetry Σ for π^0 and η photoproduction

- on the proton at $E_\gamma = 9$ GeV,” *Phys. Rev.* **C95** no. 4, (2017) 042201, [arXiv:1701.08123](#) [nucl-ex].
- [59] T. Fujiwara, T. Kugo, H. Terao, S. Uehara, and K. Yamawaki, “Nonabelian Anomaly and Vector Mesons as Dynamical Gauge Bosons of Hidden Local Symmetries,” *Prog. Theor. Phys.* **73** (1985) 926.
- [60] R. Machleidt, K. Holinde, and C. Elster, “The Bonn Meson Exchange Model for the Nucleon Nucleon Interaction,” *Phys. Rept.* **149** (1987) 1–89.
- [61] V. Mathieu, G. Fox, and A. P. Szczepaniak, “Neutral Pion Photoproduction in a Regge Model,” *Phys. Rev.* **D92** no. 7, (2015) 074013, [arXiv:1505.02321](#) [hep-ph].
- [62] NA62 Collaboration, C. Lazzeroni *et al.*, “Study of the $K^\pm \rightarrow \pi^\pm \gamma \gamma$ decay by the NA62 experiment,” *Phys. Lett.* **B732** (2014) 65–74, [arXiv:1402.4334](#) [hep-ex].
- [63] KTeV Collaboration, E. Abouzaid *et al.*, “Final Results from the KTeV Experiment on the Decay $K_L \rightarrow \pi^0 \gamma \gamma$,” *Phys. Rev.* **D77** (2008) 112004, [arXiv:0805.0031](#) [hep-ex].
- [64] S. Gori, G. Perez and K. Tobiaka noted that an additional bound can be derived from $K^+ \rightarrow \pi^+ \pi^0$ followed by $a\text{-}\pi^0$ mixing. We have derived this bound taking $\langle a\pi^0 \rangle$ from Ref. [31] and using the kaon-decay data as in Refs. [14, 62].
- [65] GlueX Collaboration, M. Dugger *et al.*, “A study of meson and baryon decays to strange final states with GlueX in Hall D (A proposal to the 39th Jefferson Lab Program Advisory Committee),” [arXiv:1210.4508](#) [hep-ex].

Photoproduction of axion-like particles

Supplemental Material

Daniel Aloni, Cristiano Fanelli, Yotam Soreq, and Mike Williams

I. ALP PRIMAKOFF PRODUCTION

This section considers the ALP Primakoff production process shown in Fig. 1 (top)

$$\gamma(k_\gamma) + N(k_N) \rightarrow a(p_a) + X(p_X), \quad (\text{S1})$$

where N is a nucleus at rest and X is a generic final state with invariant mass m_X . We begin by defining the kinematical variables, and then explore the quasi-elastic (QE) production on a heavy nuclear target, and the limiting cases of elastic production on both a heavy nuclear target and on a proton target.

A. Kinematics

The momenta in the lab frame are

$$k_\gamma = (k, 0, 0, k), \quad (\text{S2})$$

$$k_N = (m_N, 0, 0, 0), \quad (\text{S3})$$

$$p_a = \left(p, \sin\theta\sqrt{p^2 - m_a^2}, 0, \cos\theta\sqrt{p^2 - m_a^2} \right), \quad (\text{S4})$$

$$p_X = k_N + k_\gamma - p_a, \quad (\text{S5})$$

where θ is the scattering angle. The transferred momentum is

$$q = k_\gamma - p_a = (\omega, \vec{q}). \quad (\text{S6})$$

We use the standard Mandelstam variables

$$s = (k_\gamma + k_N)^2 = (p_a + p_X)^2 = m_N^2 + 2m_N k, \quad (\text{S7})$$

$$t = (k_\gamma - p_a)^2 = (k_N - p_X)^2, \quad (\text{S8})$$

$$u = (k_\gamma - p_X)^2 = (p_a - k_N)^2, \quad (\text{S9})$$

with $u + t + s = m_a^2 + m_N^2 + m_X^2$. By using the above definitions we get that

$$m_X^2 = (k_N + q)^2 = m_N^2 + 2m_N\omega + t \geq m_N^2. \quad (\text{S10})$$

The elastic limit is $m_X^2 = m_N^2$.

B. Quasi-elastic double differential cross section

We start from the most general case of Primakoff quasi-elastic production on a heavy nucleus. The generic structure of the amplitude can be written as

$$i\mathcal{M} = e \frac{c_\gamma}{\Lambda} \frac{1}{t} J_{\text{had}}^\mu J_{\gamma-a,\mu}, \quad (\text{S11})$$

where $J_{\text{had}}^\mu (J_{\gamma-a,\mu})$ is the hadronic (γ -ALP) current. The spin averaged squared amplitude is given by

$$|\overline{\mathcal{M}}|^2 = e^2 \frac{c_\gamma^2}{\Lambda^2} \frac{1}{t^2} L_{\mu\nu} W^{\mu\nu}. \quad (\text{S12})$$

Above, we adopt the standard parameterization of the hadronic tensor (see, for example, Ref. [47]),

$$W^{\mu\nu} = \sum_{\text{had,avg}} J_{\text{had}}^{\mu*} J_{\text{had}}^{\nu} = -\widetilde{W}_1 \left(g^{\mu\nu} - \frac{q^\mu q^\nu}{t} \right) + \widetilde{W}_2 V_i^\mu V_i^\nu, \quad (\text{S13})$$

where the response functions \widetilde{W}_1 (\widetilde{W}_2) are only functions of t and $x = -\frac{t}{2q \cdot k_N}$, the Bjorken parameter (or, alternatively, m_X^2), and

$$V_i^\mu = \frac{1}{m_N} \left[k_N^\mu - \frac{q \cdot k_N}{t} q^\mu \right] = \frac{1}{m_N} \left[k_N^\mu + \frac{q^\mu}{2x} \right]. \quad (\text{S14})$$

The ALP production tensor can be calculated perturbatively using the effective interaction of Eq. (1), which gives¹

$$L^{\mu\nu} = -\frac{1}{8} (t - m_a^2)^2 g^{\mu\nu} - \left(\frac{t - m_a^2}{4} \right) (k_\gamma^\mu p_a^\nu + k_\gamma^\nu p_a^\mu) - \frac{m_a^2}{2} k_\gamma^\nu k_\gamma^\mu. \quad (\text{S15})$$

Finally, the double differential cross section is given by

$$\frac{d^2\sigma}{dm_X^2 dt} = \frac{-t}{2(t + m_N^2 - m_X^2)^2} \frac{d^2\sigma}{dx dt} = \frac{1}{(s - m_N^2)^2} \frac{|\overline{\mathcal{M}}|^2}{16\pi}. \quad (\text{S16})$$

The integration boundaries are

$$m_X^2 \in [m_N^2, (\sqrt{s} - m_a)^2], \quad t_0(t_1) = \left[\frac{m_X^2 - m_a^2 - m_N^2}{2\sqrt{s}} \right]^2 - (k_{\text{cm}} \mp p_{\text{cm}})^2, \quad (\text{S17})$$

with

$$k_{\text{cm}} = \frac{km_N}{\sqrt{s}}, \quad p_{\text{cm}} = \sqrt{\left(\frac{s + m_a^2 - m_X^2}{2\sqrt{s}} \right)^2 - m_a^2}. \quad (\text{S18})$$

We estimate the nuclear response functions $\widetilde{W}_{1,2}$ in terms of the single nucleon response functions $W_{1,2}$ using the relativistic Fermi gas model as in Ref. [48] and the normalization of Ref. [47]:

$$W_T = m_N R_T = - \left(g_{ij} + \frac{q_i q_j}{|\vec{q}|^2} \right) W^{ij}, \quad W_L = m_N R_L = W^{00}. \quad (\text{S19})$$

The transverse and longitudinal response functions are related to those of Eq. (S13) via

$$W_T = 2\widetilde{W}_1, \quad W_L = -\widetilde{W}_1 \left(1 - \frac{t}{4x^2 m_N^2} \right) + \widetilde{W}_2 \left(1 - \frac{t}{4x^2 m_N^2} \right)^2. \quad (\text{S20})$$

By using the above definition of ρ and inverting these relations we find

$$\widetilde{W}_1 = \frac{1}{2} W_T, \quad \widetilde{W}_2 = \rho^2 W_L + \frac{\rho}{2} W_T. \quad (\text{S21})$$

The above equation should be understood to be the sum of the neutron and proton response functions,

$$W_{T,L} = W_{T,L}^{(n)} + W_{T,L}^{(p)}. \quad (\text{S22})$$

The explicit forms of the longitudinal and transverse response functions are

$$W_{L,T}^{(a)} = \frac{3m_N \mathcal{N}^{(a)}}{4m_p \kappa \eta_F^3} (\epsilon_F - \Gamma) \theta(\epsilon_F - \Gamma) \times \begin{cases} \frac{\kappa^2}{\tau} \left\{ \left[(1 + \tau) W_2^{(a)}(\tau) - W_1^{(a)}(\tau) \right] + W_2^{(a)}(\tau) \Delta \right\} & \text{for L} \\ 2W_1^{(a)}(\tau) + W_2^{(a)}(\tau) \Delta & \text{for T} \end{cases}. \quad (\text{S23})$$

¹ This formalism is well known for the case of electron scattering, with the trivial replacements $c_\gamma/\Lambda \rightarrow e$, and $L^{\mu\nu} = 2(k^\mu p^\nu + k^\nu p^\mu - g^{\mu\nu}(k \cdot p - m_e^2))$, see Ref. [47] for further details.

Above, the superscript $a = p(n)$ stands for protons (neutrons) in the gas, $m_p \approx m_n$ is the proton (neutron) mass, $\mathcal{N}^{(p)} = Z$, and $\mathcal{N}^{(n)} = A - Z$. We also define the dimensionless parameters

$$\kappa = \frac{|\vec{q}|}{2m_p} = \frac{1}{2m_p} \sqrt{-\frac{t}{\rho}}, \quad (\text{S24})$$

$$\lambda = \frac{\omega}{2m_p} = -\frac{t}{4xm_p m_N}, \quad (\text{S25})$$

$$\tau = \kappa^2 - \lambda^2 = -\frac{t}{4m_p^2}, \quad (\text{S26})$$

$$\eta_F = \frac{p_F}{m_p}, \quad (\text{S27})$$

$$\varepsilon_F = \sqrt{1 + \eta_F^2}, \quad (\text{S28})$$

where $p_F \approx m_p/4 \approx 235$ MeV is the Fermi momentum [48] and

$$\Gamma = \max \left[\varepsilon_F - 2\lambda, \kappa \sqrt{1 + \frac{1}{\tau}} - \lambda \right], \quad (\text{S29})$$

$$\Delta = \frac{\tau}{\kappa^2} \left[\frac{1}{3} (\varepsilon_F^2 + \varepsilon_F \Gamma + \Gamma^2) + \lambda (\varepsilon_F + \Gamma) + \lambda^2 \right] - (1 + \tau). \quad (\text{S30})$$

Finally, the single nucleon response functions are related to the Sachs form factors Eqs. (S32)–(S33) by [48]

$$W_1^{(a)}(\tau) = \tau \left[G_M^{(a)}(\tau) \right]^2, \quad W_2^{(a)}(\tau) = \frac{1}{1 + \tau} \left\{ \left[G_E^{(a)}(\tau) \right]^2 + \tau \left[G_M^{(a)}(\tau) \right]^2 \right\}, \quad (\text{S31})$$

where the Sachs form factors are given by [36, 37]

$$G_E^p(t) = \frac{1}{(1 - t/q_0^2)^2}, \quad (\text{S32})$$

$$G_M^p(t) = \frac{\mu_p}{(1 - t/q_0^2)^2}, \quad (\text{S33})$$

$$G_E^n(t) = \frac{-t}{4m_p^2} \frac{\mu_n}{(1 - t/q_0^2)^2} \frac{1}{1 - 5.6t/m_p^2} \approx 0, \quad (\text{S34})$$

$$G_M^n(t) = \frac{\mu_n}{(1 - t/q_0^2)^2}, \quad (\text{S35})$$

with $\mu_p = 2.793$ ($\mu_n = -1.913$) [38] the magnetic moment of the proton (neutron) and $q_0^2 = 0.71$ GeV². The resulting QE cross section is given by

$$\frac{d^2 \sigma_{\gamma N \rightarrow aX}^{\text{QE}}}{dt dx} = \frac{\alpha g_{a\gamma}^2}{32\Lambda^2} \frac{w_1 \widetilde{W}_1 + w_2 \widetilde{W}_2}{m_N^2 t x^2 (m_N^2 - s)^2}, \quad (\text{S36})$$

where

$$w_1 = 2m_N^2 (m_a^2 - t)^2, \quad (\text{S37})$$

$$w_2 = m_N^2 m_a^2 (2t - m_a^2) - t [(s - m_N^2)^2 + t m_N^2] - \frac{t}{x} (s - m_N^2)(t - m_a^2). \quad (\text{S38})$$

C. Elastic scattering limit

Elastic scattering corresponds to the following limit (see discussion in Ref. [47]):

$$m_X^2 = m_N^2 \quad \Rightarrow \quad \omega = -\frac{t}{2m_N} \quad \Rightarrow \quad x = 1. \quad (\text{S39})$$

The nuclear response function is obtained by integrating Eq. (S13), which gives

$$F_{\mu\nu}^{\text{had}} = 16\pi m_N^2 \left(-F_1^2 \left(g^{\mu\nu} - \frac{q^\mu q^\nu}{t} \right) + F_2^2 V_i^\mu V_i^\nu \right), \quad (\text{S40})$$

and

$$F_1^2 = \frac{F_T^2}{2}, \quad F_2^2 = \frac{\rho}{2} (F_T^2 + 2\rho F_L^2). \quad (\text{S41})$$

The transverse and longitudinal response functions are approximately

$$F_T^2(t) \simeq 0, \quad F_L^2(t) \simeq \frac{Z^2}{4\pi} F_0^2(t), \quad (\text{S42})$$

where

$$F_0(t) = \frac{1}{Z} \int d^3x \frac{\sin(|\vec{q}|x)}{|\vec{q}|x} \rho(x)_{00}, \quad \rho(x)_{00} = \frac{\rho_0}{1 + \exp\left(\frac{x-R}{a}\right)}. \quad (\text{S43})$$

Above, $|\vec{q}| = \sqrt{t(4m_N^2 - 1)}$, a and R are determined from data using the two parameter Fermi model (see Ref. [49]). Finally, ρ_0 is defined by the normalization condition $\int d^3x \rho(x)_{00} = Z$. Therefore, the amplitude squared is

$$|\overline{\mathcal{M}}|^2 = 2\pi \frac{8e^2 g_{\text{lep}}^2}{t^2} \rho^2 L^{\mu\nu} \left(k_N^\mu + \frac{q^\mu}{2} \right) \left(k_N^\nu + \frac{q^\nu}{2} \right) \frac{Z^2}{4\pi} F_0^2(q), \quad (\text{S44})$$

and the elastic cross section is

$$\frac{d\sigma}{dt} = \frac{|\overline{\mathcal{M}}|^2}{64\pi s k_{\text{cm}}^2}, \quad (\text{S45})$$

where the integration boundaries are given in Eq. (S17) for $m_X = m_N$ and k_{cm} is defined in Eq. (S18). The resulting elastic cross section is

$$\frac{d\sigma_{\gamma N \rightarrow aN}^{\text{El}}}{dt} = 2\alpha Z^2 \frac{g_{a\gamma}^2}{\Lambda^2} \frac{m_N^4 \left(m_a^2 t (m_N^2 + s) - m_a^4 m_N^2 - t \left((m_N^2 - s)^2 + st \right) \right)}{t^2 (m_N^2 - s)^2 (t - 4m_N^2)^2} F_0^2(q). \quad (\text{S46})$$

D. Proton target

A simple case is a proton target, where we consider elastic scattering. The proton effective vertex is

$$\mathcal{L}_{\text{eff}-p} = e\bar{\psi}_p \left(\gamma_\mu F_1^p(t) + \frac{i\sigma_{\mu\nu}}{2m_p} F_2^p(t) q^\nu \right) \psi_p, \quad (\text{S47})$$

where

$$F_1^p(t) = \frac{4m_p^2 G_E^p(t) - t G_M^p(t)}{4m_p^2 - t}, \quad F_2^p(t) = \frac{4m_p^2 (G_M^p(t) - G_E^p(t))}{4m_p^2 - t}. \quad (\text{S48})$$

and $G_{E,M}^p$ are given in Eqs. (S32) and (S33). The cross section is

$$\frac{d\sigma_{\gamma p \rightarrow ap}}{dt} = \frac{\alpha g_{a\gamma}^2}{32\Lambda^2} \frac{f_1 F_1^{p,2}(t) + f_{12} F_1^p(t) F_2^p(t) + f_2 F_2^{p,2}(t)}{m_p^2 t^2 (m_p^2 - s)^2}, \quad (\text{S49})$$

with

$$f_1 = 2m_p^2 \{ 2m_a^2 t (m_p^2 + s + t) - m_a^4 (2m_p^2 + t) - t [2(m_p^2 - s)^2 + 2st + t^2] \}, \quad (\text{S50})$$

$$f_2 = t \{ t [m_p^4 - 2m_p^2 (s + t) + s(s + t)] + t m_a^2 (3m_p^2 - s) - m_a^4 m_p^2 \}, \quad (\text{S51})$$

$$f_{12} = 4m_p^2 t (m_a^2 - t)^2. \quad (\text{S52})$$

E. Quasi-Elastic data-driven signal estimation

The ALP Primakoff signal is proportional to the Primakoff production yield of π^0 , η or η' . Therefore, by measuring these yields for different s , t , and x one can perform data-driven signal estimation and normalize the ALP search to the data without relying on theory inputs for the form factors. In addition, the experimental photon flux does not need to be known, and only the response of the detector at m_a relative to m_P is required. Here, we discuss the general case of quasi-elastic scattering on a heavy nucleus. The elastic case is discussed in the Letter. In principle, this method can also be used to perform a measurement of the $\Gamma_{\eta^{(\prime)} \rightarrow \gamma\gamma} / \Gamma_{\pi^0 \rightarrow \gamma\gamma}$ ratio with reduced hadronic uncertainties.

For a given target, N , the ratio between ALP and $P = \pi^0, \eta, \eta'$ Primakoff production is

$$\begin{aligned} \mathcal{R}_{aP}(s, t, x, m_a, m_P) &= \left(\frac{d\sigma_{\gamma N \rightarrow aX}}{dtdx} \right) / \left(\frac{d\sigma_{\gamma N \rightarrow PX}}{dtdx} \right) \\ &= \frac{g_{a\gamma}^2 / \Lambda^2}{64\pi \Gamma_{P \rightarrow \gamma\gamma} / m_P^3} \frac{(m_a^2 - t)^2}{(m_P^2 - t)^2} \frac{1 + w_{21}(s, t, x, m_a) W_{21}(t, x)}{1 + w_{21}(s, t, x, m_P) W_{21}(t, x)}, \end{aligned} \quad (\text{S53})$$

with

$$W_{21}(t, x) = \widetilde{W}_2(t, x) / \widetilde{W}_1(t, x), \quad w_{21}(s, t, x, m_a) = w_2 / w_1. \quad (\text{S54})$$

From Eq. (S53) we see that in order to normalize ALP production to pseudoscalar production one needs to know W_{21} . This can be achieved by measuring the differential cross section at two different s values:

$$\begin{aligned} \mathcal{R}_{PP}(s_1, s_2, t, x, m_P) &= \left(\frac{d\sigma_{\gamma N \rightarrow PX}}{dtdx} \right)_{s=s_1} / \left(\frac{d\sigma_{\gamma N \rightarrow PX}}{dtdx} \right)_{s=s_2} \\ &= \frac{1 + w_{21}(s_1, t, x, m_P) W_{21}(t, x) (m_N^2 - s_2)^2}{1 + w_{21}(s_2, t, x, m_P) W_{21}(t, x) (m_N^2 - s_1)^2}, \end{aligned} \quad (\text{S55})$$

which allows us to determine $W_{21}(t, x)$ and estimate the ALP Primakoff production cross section. We note that this should be done on the data around the Primakoff peak where strong pseudoscalar-meson production can be neglected.

II. ALP STRONG PHOTOPRODUCTION

In the Letter, we used an approximation to obtain the data-driven normalization for strong ALP photoproduction. This was because, as discussed in Ref. [58], η production at GLUEX energies, while clearly dominantly t -channel, is not yet fully understood. Here, we show that—once both π^0 and η photoproduction are well understood—it is possible to derive a fully data-driven normalization strategy similar to the one we proposed above for Primakoff production.

We estimate this contribution using the vector-meson-dominance (VMD) model. The process begins with an insertion of γ - ρ (γ - ω) mixing, an interaction of the form $PV V^{(\prime)}$ where $P = \pi, \eta, \eta'$ or $P = a$ for the ALP and $V = \rho, \omega$ (see Ref. [59] and the Supplemental Material of Ref. [31] for further details). The ALP-gluon coupling can be replaced by an ALP $U(3)$ representation by performing a chiral transformation of the light-quark fields [32–34]. Following Ref. [31], we denote this as \mathbf{a} and take this m_a -dependent representation directly from Ref. [31].

For the photon-meson mixing we define

$$\gamma_\rho = 3\gamma_\omega = e/g \approx 4.9 \times 10^{-2}, \quad (\text{S56})$$

where $g \approx \sqrt{12\pi}$ is the VMD coupling [59]. As this factor is already at the percent level, we do not consider more than a single insertion. For the ρ and ω couplings to the proton, we follow Ref. [60]. Comparing to our notations of the $F_{1,2}$ form-factors in Eq. (S47) we have

$$eF_1^\rho \rightarrow g_{\rho NN} \approx 3.25, \quad (\text{S57})$$

$$eF_2^\rho \rightarrow g_{\rho NN} \kappa_{\rho NN} \approx 20.7, \quad (\text{S58})$$

$$eF_1^\omega \rightarrow g_{\omega NN} \approx 15.9, \quad (\text{S59})$$

$$eF_2^\omega \rightarrow g_{\omega NN} \kappa_{\omega NN} \approx 0. \quad (\text{S60})$$

The $\gamma p \rightarrow ap$ cross section from γ - V_1 mixing and t -channel exchange of V_2 , including the interference with γ - V_1 mixing and t -channel exchange of $V_{2'}$, is given by

$$\frac{d\sigma}{dt} = \sum_{V_i=\rho,\omega} \frac{\gamma_{V_1} \gamma_{V_1'} g_{aV_1 V_2} g_{aV_1' V_2'} g_{V_2 NN} g_{V_2' NN}}{128\pi} \mathcal{P}_{V_2} \mathcal{P}_{V_2'}^* \frac{f_1 + f_{12} (\kappa_{V_2' NN} + \kappa_{V_2 NN}) / 2 + f_2 \kappa_{V_2 NN} \kappa_{V_2' NN}}{m_p^2 (m_p^2 - s)^2}, \quad (\text{S61})$$



FIG. S1: Schematic of the PRIMEX experiment (not to scale) including the high-resolution multichannel calorimeter (HYCAL) which is vital to the search proposed here.

PRIMEX run	target	thickness [X_0]	integrated luminosity [1/pb]	beam energy [GeV]
I	^{12}C	5%	0.3	4.9–5.5
I	^{208}Pb	5%	0.002	4.9–5.5
II	^{12}C	8%	0.4	4.4–5.3
II	^{28}Si	10%	0.3	4.4–5.3

TABLE S1: PRIMEX data-taking conditions in both experimental runs.

where $f_{1,2,12}$ are given in Eqs. (S50)–(S52). The Regge propagator, $\mathcal{P}_V(t)$, replacing the vector meson Breit-Wigner propagator is

$$\mathcal{P}_V(t) = \frac{\pi}{\Gamma(\alpha(t))} \frac{1 - e^{-i\pi\alpha(t)}}{2 \sin(\pi\alpha(t))} \left(\frac{s}{\text{GeV}^2} \right)^{\alpha(t)-1}, \quad (\text{S62})$$

with $\alpha_V(t) = \alpha_V^0 + \alpha'_V t$, with $\alpha_V^0 = 0.5$, $\alpha'_V = 0.9 \text{ GeV}^{-2}$ [61]. Finally, the ALP–vector-meson coupling in Eq. (S61) is given by

$$g_{aV_1 V_2} = -\frac{3g^2}{8\pi^2 f_a} \langle \mathbf{a} \mathbf{V}_1 \mathbf{V}_2 \rangle, \quad (\text{S63})$$

where $\langle \mathbf{a} \mathbf{V}_1 \mathbf{V}_2 \rangle$ is the ALP–vector–vector effective interaction, see Ref. [31] (for a pseudoscalar meson, \mathbf{a} is replaced by the appropriate $U(3)$ representation, and $f_a \rightarrow f_\pi$). Under the assumption that this model adequately describes both π^0 and η production, it is straightforward to obtain the ratio of the ALP and $P = \pi^0, \eta$ differential cross sections from the equations above and perform a fully data-driven normalization similar to what we proposed for Primakoff production. Similarly, this same procedure can be followed for any other pseudoscalar-meson photoproduction model.

To estimate the accuracy of the approximation made in the Letter, we assume that the model described above is valid for both π^0 and η photoproduction. To be conservative, we allow for an arbitrary phase between the ρ and ω exchange amplitudes, and choose its value to maximize the discrepancy induced by the approximation used in the Letter. We find that the largest error is less than a factor of 2, and as expected, occurs near 0.4 GeV where $\langle \mathbf{a} \pi^0 \rangle$ and $\langle \mathbf{a} \eta \rangle$ are roughly equal in size.

III. PRIMEX DETAILS

This section describes the PRIMEX experiment and data-taking conditions, along with the details of our toy PRIMEX Monte Carlo simulation and our bump hunt of the published $m_{\gamma\gamma}$ spectrum from one angular bin of carbon-target data in Ref. [30].

A. PRIMEX Description

The first run of the PRIMEX experiment was in Hall B at Jefferson Lab in 2004 [30]. Data were collected on both C and Pb targets using a 4.9–5.5 GeV photon beam and a high-resolution multichannel calorimeter. The integrated luminosities were 0.3/pb for C and 0.002/pb for Pb. A follow-up run of PRIMEX was performed in 2010, which collected 0.4/pb on C and 0.3/pb on Si. The target and beam properties for each run are given in Table S1. The PRIMEX calorimeter was located 7.5 m downstream of the targets with an acceptance covering $\approx 1 \text{ m}^2$. A 4.1 cm \times 4.1 cm square hole was left at the center to allow the beam to pass through. This calorimeter geometry provides good acceptance for $0.03 \lesssim m_a \lesssim 0.3 \text{ GeV}$. We developed a simple toy Monte Carlo of this set up, including the acceptance, efficiency, and resolution of the calorimeter taken from Refs. [45, 46].

Ref. [30] used the following selection to measure $\Gamma_{\pi^0 \rightarrow \gamma\gamma}$ (we adopt this selection for the ALP search): the incident photon energy had to be in the range 4.9–5.5 GeV; the sum of the two decay photon energies was required to be larger than 2.5 GeV; and the *elasticity*, defined as the sum of the two decay photon energies divided by the photon beam energy, had to be within 3 times the resolution of unity. The product of the acceptance and efficiency is $\gtrsim 30\%$ in the region $0.03 < m_a < 0.3$ GeV, but drops quickly outside of this region due to the acceptance. We find that the resolution should be $\approx 0.02 \times m_a$ in this region, which agrees with the value of $0.017 \times m_{\pi^0}$ found in Ref. [30].

To estimate the sensitivity of each PRIMEX data sample, we need to determine the mass dependence of the efficiency and to estimate the background versus $m_{\gamma\gamma}$ in each sample. Using the known nuclear form factors and Primakoff differential cross section [47–49], we generate Primakoff π^0 Monte Carlo events for the PRIMEX photon-beam energy. We require that both photons from the $\pi^0 \rightarrow \gamma\gamma$ decay are in the PRIMEX calorimeter fiducial acceptance region and apply the required smearing to account for resolution. We then apply the full selection of Ref. [30] and find that our predicted π^0 Primakoff yields are consistent with those observed in Refs. [50, 51]. We assume that the reconstruction efficiency is independent of the ALP mass in the search region (excluding geometrical acceptance effects). In addition, we assume that the ALP bump hunt will only use candidates with $\theta_{\gamma\gamma} < 0.5^\circ$, where π^0 production is dominated by the Primakoff process for all targets. We determine the efficiency at each m_a using our toy Monte Carlo and these selection criteria.

Obtaining a data-driven background estimate will be straightforward for the PRIMEX collaboration using the $m_{\gamma\gamma}$ sidebands at each m_a (see, *e.g.*, Refs. [52, 53]). However, estimating the background for this study—without access to the data—is considerably more difficult. We considered many possible backgrounds, *e.g.* $\gamma N \rightarrow N\omega(\pi^0[\gamma\gamma]\gamma)$ where one photon is not reconstructed or the π^0 photons are merged into a single cluster, though we found that no hadronic reactions are capable of contributing background at a rate comparable to that observed in Fig. 2 of Ref. [30]. Therefore, we conclude that the PRIMEX background is dominantly due to electromagnetic interactions of the photon beam with the target that produce either additional photons or e^+e^- pairs. Figure 2 of Ref. [30] shows the forward-most angular region. Given that the beam backgrounds should decrease moving away from the beam line, using this angular bin—and assuming a uniform $\theta_{\gamma\gamma}$ distribution—provides a conservative background estimate. We also conservatively assume that the backgrounds above (below) the $m_{\gamma\gamma}$ region shown in Fig. 2 take on the values at the upper (lower) edge of the plot, even though they appear to be decreasing in both directions (which is expected). The resulting predicted background—excluding the π^0 peak region—is between 40 and 300 candidates per $\pm 2\sigma$ window for the first PRIMEX carbon-target run. We scale the beam-induced background, which is shown for the first C run, by the product of the target radiation length and the number of photons on target for each PRIMEX run (see Table S1).

B. Bump Hunt of Fig. 2 of Ref. [30]

Ref. [30] published the diphoton mass spectrum near the π^0 peak for one forward angular bin from the C data obtained in the first PRIMEX run (see Fig. 2 of Ref. [30]). We have digitized this plot (see Fig. S2). We scan the $m_{\gamma\gamma}$ spectrum in steps of roughly half the resolution (1 MeV steps). At each mass, a binned maximum likelihood fit is performed to the data in Fig. S2. The profile likelihood is used to determine the confidence interval of the number of $a \rightarrow \gamma\gamma$ decays observed, from which an upper limit at 95% confidence level is obtained. The confidence intervals are defined using the *bounded likelihood* approach, which involves taking the change in the likelihood relative to zero signal, rather than the best-fit value, if the best-fit signal value is negative. This enforces that only physical (nonnegative) upper limits are placed on the ALP yield, and prevents defining exclusion regions that are much better than the experimental sensitivity in cases where a large deficit in the background yield is observed.

The fit model contains contributions from $\pi^0 \rightarrow \gamma\gamma$, combinatorial diphoton combinations, a broad peak-like structure below the π^0 mass, and an $a \rightarrow \gamma\gamma$ signal component. The π^0 contribution is described by a double Gaussian function, where both Gaussians share the same mean. The combinatorial background is modeled by the *ad hoc* function $(c_0 + c_1 m_{\gamma\gamma}) \times (1 - \exp\{c_2(m_{\gamma\gamma} - c_3)\})$ (the c_i are free parameters in the fit), which is observed to describe the data well. There is a broad peak-like structure in the background below the π^0 mass. We model this contribution using a single wide Gaussian. Finally, the signal is modeled using the same PDF as that of the π^0 except, of course, for the value of the mean mass which is fixed for each test mass value. Figure S2 shows the $m_{\gamma\gamma}$ spectrum fit to the background-only model, which describes the data well. The observed π^0 yield is ≈ 5100 . The constraints on c_γ/Λ are obtained from the upper limit on the number of $a \rightarrow \gamma\gamma$ decays observed at each m_a as described above. These are shown in Fig. S2 compared to their expected values. Near 115 and 160 MeV, these are the best limits set to date on the ALP-photon coupling. The sensitivity using the full PRIMEX data set—rather than just one angular region of the C data—is expected to be substantially better, and will cover a much larger mass region.

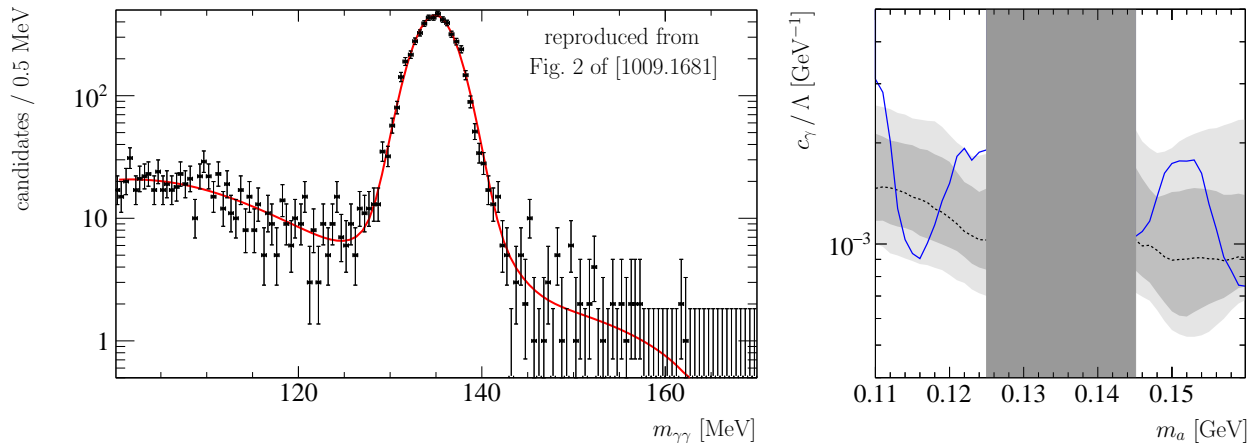


FIG. S2: (left) Reproduction of Fig. 2 of Ref. [30] fit to the background-only model described in the text. (right) Limits obtained from (solid blue) our bump hunt of this $m_{\gamma\gamma}$ distribution compared with the (dashed) expected, (dark shaded) $\pm 1\sigma$, and (light shaded) $\pm 2\sigma$ regions.

IV. GLUEX DETAILS

This section describes the GLUEX experiment and data-taking conditions, along with the details of our toy GLUEX Monte Carlo simulation and our bump hunt of the published $m_{\gamma\gamma}$ spectrum from $\approx 1/\text{pb}$ of proton-target data in Ref. [58].

A. GLUEX Description

The GLUEX experiment began taking data in Hall D at Jefferson Lab in 2016. In the spring 2016, $\approx 1/\text{pb}$ of data on a liquid-hydrogen target were collected with a linearly polarized 8.2–9.2 GeV photon beam. These data were used to measure the beam asymmetry Σ for both π^0 and η photoproduction [58]. The experiment has collected $\approx 50/\text{pb}$ thus far, and plans to collect $\mathcal{O}(1/\text{fb})$ of data using its nominal liquid-hydrogen target [65]. GLUEX has both forward and central calorimeters. We take the GLUEX acceptance, efficiency, and resolution from Refs. [56, 57]. The most important component of the GLUEX detector to our studies is the forward calorimeter, which is located about 5.6 m downstream of the target and covers roughly from 2 to 11° in the lab frame. Its resolution is roughly $3.5\% + 5.7\%/\sqrt{E_\gamma/\text{GeV}}$.

An updated version of the PRIMEX experiment recently ran using the GLUEX detector with an additional small-angle calorimeter [54]. This new experiment used a helium target, which makes it less sensitive than PRIMEX for ALPs; however, several proposals have been made for future GLUEX running with heavy nuclear targets [55]. Specifically, we consider a Pb target here, though other targets are possible and it is simple to rescale our results for other nuclei. We take the acceptance, efficiency, and resolution for the small-angle calorimeter from Ref. [54]. The small-angle calorimeter is located about 4 m downstream of the nominal GLUEX forward calorimeter, and fully covers the acceptance hole in the nominal GLUEX forward calorimeter. As was done for PRIMEX, a $4.1\text{ cm} \times 4.1\text{ cm}$ square hole was left at the center to allow the beam to pass through.

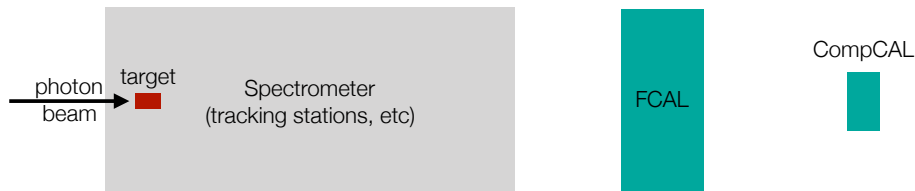


FIG. S3: Schematic of the GLUEX experiment (not to scale) including the forward (FCAL) and an additional small-angle (CompCAL) calorimeters, which are vital to the search proposed here.

For $m_a < m_\eta$, we rescale the expected beam background from the PRIMEX Pb run. There are three additional backgrounds that contribute to the GLUEX run at higher masses: Primakoff production of η and η' mesons, and coherent nuclear production of $\gamma N \rightarrow N\omega(\pi^0[\gamma\gamma]\gamma)$. The cross sections for these processes are well known, making it straightforward to estimate their yields using Monte Carlo. That said, these backgrounds are peaking, so we exclude the η and η' regions, and apply a relative 1% systematic uncertainty on the background yield between the η and η' masses. This systematic is the dominant effect in our prediction of the sensitivity in this mass region (this can likely be reduced in an actual search, improving the sensitivity greatly). The GLUEX experiment could explore regions of ALP parameter space where the ALP flight distance becomes nonnegligible. Using Monte Carlo, we estimate that the impact on the ALP mass resolution and acceptance is small provided that its lab-frame flight distance is $\lesssim 30$ cm (the length of the nominal liquid hydrogen target cell). For simplicity, we apply a fiducial cut on the flight distance at 30 cm, which is conservative since ALPs that decay after this distance could still be detected and a detailed study could determine the appropriate signal shape for each value of Λ . We show projections for 2 luminosity values, though again it is easy to rescale these projections for other values. The smaller data set corresponds to collecting 1/pb of Pb-target data. The larger data set assumes that as much data is collected on a Pb target as is expected in the full GLUEX proton-target run. A more likely scenario would involve collecting a total nuclear-target data sample of roughly this size that consists of several smaller samples using different nuclei. If this is the case, combining these samples using our data-driven approach is simple and the total sensitivity would be an $\mathcal{O}(1)$ factor worse than collecting only Pb data.

B. Bump Hunt of Fig. 3 of Ref. [58]

Ref. [58] published the $m_{\gamma\gamma}$ spectrum (see Fig. 3 of Ref. [58]), along with the yields and efficiencies versus t of both the π^0 and η mesons (see Fig. 4 of Ref. [58]). We have digitized Fig. 3 (see Fig. S4). We use this data to place constraints on c_g/Λ using Eq. (6). The ALP decay branching fraction is taken from Ref. [31], though it is close to unity throughout this mass range. Ref. [58] provides the efficiencies versus t at m_{π^0} and m_η . We discard the region $|t| < 0.1 \text{ GeV}^2$ because the efficiency is small and sharply varying with t . We discard the region $|t| > 1 \text{ GeV}^2$ because our approximation in Eq. (6) begins to break down here. Note that, by necessity, we keep the background from these regions, since we have no way of removing it from the $m_{\gamma\gamma}$ spectrum of Fig. 3 in Ref. [58]. We linearly interpolate the efficiencies given at each t for m_{π^0} and m_η to each m_a , and confirm this approach is valid to $\mathcal{O}(10\%)$ using toy Monte Carlo. In this toy Monte Carlo, we generate the ALPs using the Regge model discussed above and the GLUEX fiducial region described in the previous subsection; however, since the $[s, t]$ bins are small, the production model has negligible impact on obtaining the efficiencies. Additionally, the same ALP lifetime correction is applied here as is applied for the Primakoff scenario, though this is a small correction in this case.

The approach used here is the same as for our PRIMEX bump hunt. We scan the $m_{\gamma\gamma}$ spectrum in steps of 10 MeV, which is the bin width of Fig. 3 of Ref. [58]. At each mass, a binned maximum likelihood fit is performed to the data in Fig. S4. The profile likelihood is used to determine the upper limit on the number of $a \rightarrow \gamma\gamma$ decays observed using the bounded likelihood approach. The fit model contains contributions from $\pi^0 \rightarrow \gamma\gamma$, $\eta \rightarrow \gamma\gamma$, combinatorial diphoton combinations, and an $a \rightarrow \gamma\gamma$ signal component. The π^0 and η contributions are described by double Gaussian functions. The combinatorial background is modeled by a linear function. The signal is modeled using a Gaussian PDF with a relative resolution fixed to the value observed for the η peak of $\approx 3.5\% \times m_a$ (this constant relative resolution is confirmed by our toy Monte Carlo).

Figure S4 shows the $m_{\gamma\gamma}$ spectrum fit to the background-only model, which describes the data well. The constraints on c_g/Λ are obtained from the upper limit on the number of $a \rightarrow \gamma\gamma$ decays observed at each m_a as described above. These are shown in Fig. S4 compared to their expected values. Over some of this mass range, these are the best limits set to date on the ALP-gluon coupling. The sensitivity using the full GLUEX data set—roughly 1000 times more luminosity—is expected to be about $1000^{\frac{1}{4}} \approx 5$ times better.

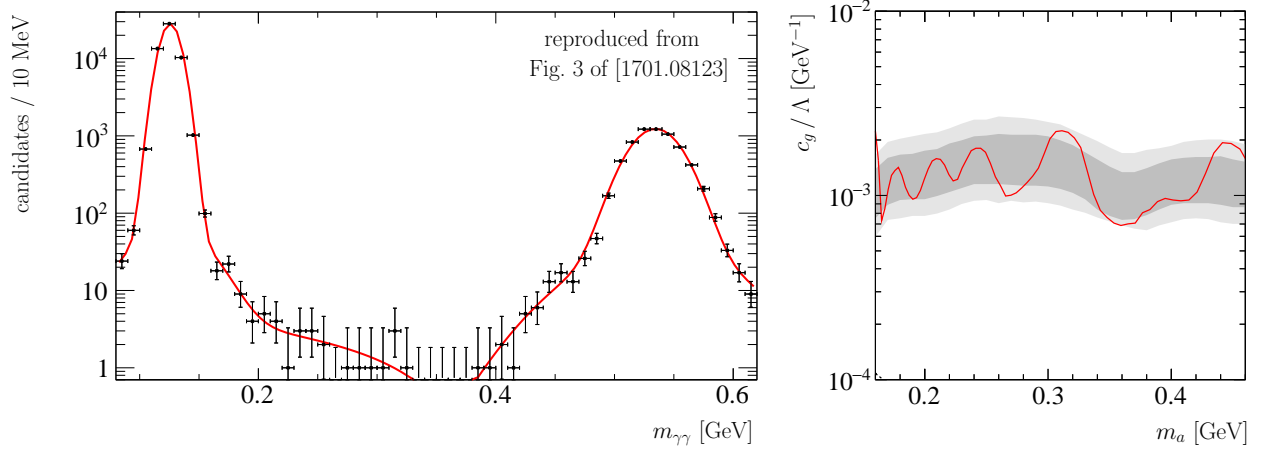


FIG. S4: (left) Reproduction of Fig. 3 of Ref. [58] fit to the background-only model described in the text. (right) Limits obtained from (solid red) our bump hunt of this $m_{\gamma\gamma}$ distribution compared with the (dashed) expected, (dark shaded) $\pm 1\sigma$, and (light shaded) $\pm 2\sigma$ regions.